GEOPHYSICAL RESEARCH LETTERS, VOL. 36, L24502, doi:10.1029/2009GL040948, 2009

Surface-melt driven Laurentide Ice Sheet retreat during the early Holocene

A. E. Carlson,[1] F. S. Anslow,[2] E. A. Obbink,[1] A. N. LeGrande,[3] D. J. Ullman,[1] and J. M. Licciardi[4]

Received 21 September 2009; revised 3 November 2009; accepted 30 November 2009; published 30 December 2009.

[1] To better understand mechanisms of ice-sheet decay, we investigate the surface mass balance of the Laurentide Ice Sheet (LIS) during the early Holocene, a period of known rapid LIS retreat. We use a surface energy-mass balance model (EMBM) driven with conditions derived from an equilibrium atmosphere-ocean general circulation model 9 kilo-years ago simulation. Our EMBM indicates a net LIS surface mass balance of -0.67 ± 0.13 m yr^{-1}, with losses primarily due to enhanced boreal summer insolation and warmer summers. This rate of loss compared to LIS volume reconstructions suggests that surface ablation accounted for 74 ± 22% of the LIS mass loss with the remaining loss likely driven by dynamics resulting in basal sliding and calving. Thus surface melting likely played a governing role in the retreat and disappearance of this ice sheet. **Citation:** Carlson, A. E., F. S. Anslow, E. A. Obbink, A. N. LeGrande, D. J. Ullman, and J. M. Licciardi (2009), Surface-melt driven Laurentide Ice Sheet retreat during the early Holocene, *Geophys. Res. Lett.*, *36*, L24502, doi:10.1029/2009GL040948.

1. Introduction

[2] During the early Holocene (~11.5–8.0 ka, kilo-years ago), enhanced boreal summer insolation relative to present warmed the Northern Hemisphere driving the retreat and ultimate disappearance of the Laurentide Ice Sheet (LIS) [*Mitchell et al.*, 1988; *Berger and Loutre*, 1991; *Pollard et al.*, 1998; *LeGrande and Schmidt*, 2009]. LIS retreat was rapid during this period, contributing to sea-level rise at rates of up to ~1.3 cm yr^{-1} [*Licciardi et al.*, 1998; *Tarasov and Peltier*, 2004; *Carlson et al.*, 2008]. This rapid loss of ice mass may reflect amplified ablation in response to enhanced summer insolation and attendant warming [*Berger and Loutre*, 1991] (Figures 1a and 1b). Alternatively, rapid LIS retreat may have arisen from dynamic ice-sheet instabilities paced by insolation, such as grounding line destabilization leading to increased calving, and/or enhanced basal sliding from meltwater lubricating the glacier bed, both of which have been recently observed on the Greenland Ice Sheet [*Zwally et al.*, 2002; *Joughin et al.*, 2004, 2008; *Luckman et al.*, 2006; *Rignot and Kanagaratnam*, 2006; *Holland et al.*, 2008; *Nick et al.*, 2009; *Pritchard et al.*, 2009; *Shepherd et al.*, 2009], though the importance of the latter mechanism is likely less than initially hypothesized [*Joughin et al.*, 2008]. The relative contributions of surface ablation and dynamics to total ice-sheet mass loss have significant implications for predictions of future sea-level rise [*Pfeffer et al.*, 2008]. Here we aim to better constrain the former by exploring the surface forcing mechanisms behind the retreat of the LIS in the early Holocene (~9 ka), a time period with Northern Hemisphere summers warmer than pre-industrial climate providing a potential analog for climate at the end of this century [*Hansen et al.*, 2007; *Meehl et al.*, 2007; *Carlson et al.*, 2008; *LeGrande and Schmidt*, 2009].

2. Energy-Mass Balance Model (EMBM)

[3] We simulate surface mass balance using the surface energy-mass balance model (EMBM) of *Anslow et al.* [2008] adapted for the LIS. This EMBM accounts for temporal and spatial changes in the physical characteristics of a melting snow or ice surface including surface roughness, albedo, and geometry relative to incoming shortwave radiation. We account for meltwater refreezing following *Huybrechts and deWolde* [1999]. We assume base albedo of snow (0.6) and ice (0.4) based on modern GIS observations [*Greuell*, 2000]. Four other more poorly constrained parameters that govern the model physics (albedo decay rate of snow and ice, and surface roughness of snow and ice) were adjusted to assess their effects on mass balance. A range of reasonable values for each parameter was chosen based on observations of the modern Greenland Ice Sheet to provide bounds for the LIS mass balance (Table 1). We performed 110 Monte Carlo sensitivity simulations, randomly varying each parameter within their appropriate ranges. Our EMBM accounts only for changes in the LIS surface ablation and accumulation. In a perfect simulation, remaining mass loss required to account for the total LIS mass loss at 9 ka is the result of ice dynamic effects, allowing an estimation of the relative roles of ice deformation, basal sliding and calving in modulating ice mass loss.

[4] The EMBM is forced by a set of climate variables (air temperature, wind speed and direction, humidity, surface shortwave radiation, downward longwave radiation, and precipitation) that are obtained from the fully-coupled atmosphere-ocean general circulation model, Goddard Institute for Space Studies ModelE-R. The ModelE-R simulation uses full 9 ka boundary conditions including a remnant LIS (including altered North American drainage basins) (Figure 2a) [*Licciardi et al.*, 1998], 40 m sea level

[1]Department of Geoscience, University of Wisconsin-Madison, Madison, Wisconsin, USA.
[2]Earth and Ocean Sciences, University of British Columbia, Vancouver, British Columbia, Canada.
[3]NASA Goddard Institute for Space Studies and Center for Climate System Research, Columbia University, New York, New York, USA.
[4]Department of Earth Sciences, University of New Hampshire, Durham, New Hampshire, USA.

0094-8276/09/2009GL040948$05.00

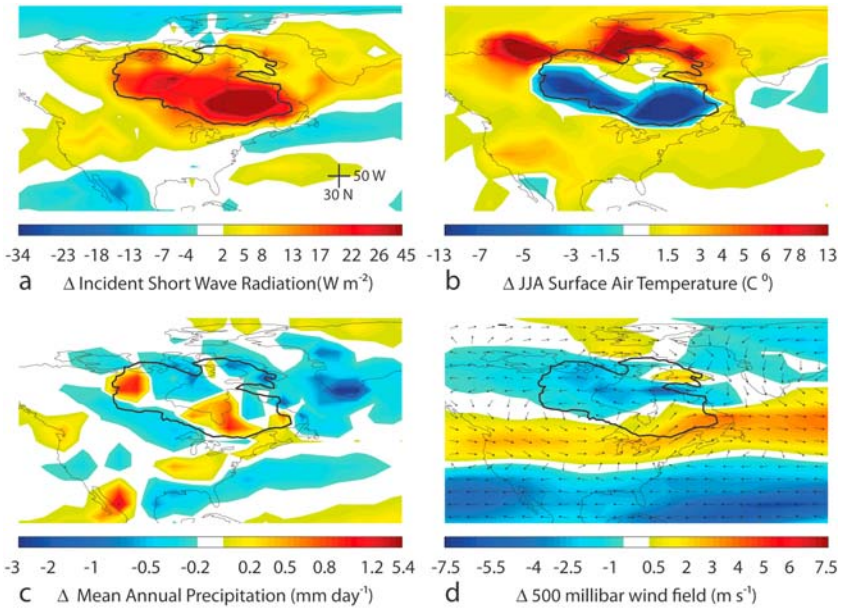

Figure 1. GISS ModelE-R 9 ka climate output relative to pre-industrial (Miller projection of map) [*LeGrande and Schmidt*, 2009]. (a) Change in incident short wave radiation. (b) Change in summer (JJA) surface air temperature. (c) Change in mean annual precipitation. (d) Change in 500 millibar jet stream strength and direction. Black lines denote the outline of the 9 ka LIS [*Licciardi et al.*, 1998; *Dyke*, 2004].

lowering (and associated changes to mean ocean salinity and $\delta^{18}O$), glacial Lake Agassiz along the southwestern LIS margin [*Dyke*, 2004], appropriate greenhouse gas levels (9 ka/Pre-industrial = CO_2:0.93, CH_4:0.83, N_2O:0.89) [*Indermühle et al.*, 1999; *Brook et al.*, 2000; *Sowers et al.*, 2003], and alterations to insolation [*Berger and Loutre*, 1991] (Figures 1a–1d) [*LeGrande and Schmidt*, 2009]. ModelE-R simulates water isotopes within the hydrologic cycle and demonstrates a significant correlation between simulated and the reconstructed 9 ka $\delta^{18}O$ of precipitation and seawater (r^2 = 0.83) [*Carlson et al.*, 2008]. The skill of the simulated northern North Atlantic regional climate is greater (r^2 = 0.89), with simulated $\delta^{18}O$ within 4% of reconstructions at 1σ. It is desirable to assess the effects different climate models may have on the EMBM [e.g., *Pollard et al.*, 2000]; this examination will occur in the future once more coupled AOGCM simulations of this time period become more readily available. Our results and discussion include only the EMBM uncertainty. While there is uncertainty in the climate forcing, the strong correlation between the simulated and reconstructed hydrologic cycle for 9 ka, particularly for the North Atlantic region, gives us confidence in the boundary conditions we have applied to the EMBM.

[5] We downscale ModelE-R variables by interpolating the simulated climate horizontally and vertically with appropriate atmospheric lapse rates for elevation-sensitive meteorological variables (e.g., -5°C km^{-1} for surface air temperature and 1 mm km^{-1} for precipitation, reliable values for ice sheets) [*Pollard et al.*, 2000; *Marshall et al.*, 2002; *Abe-Ouchi et al.*, 2007] onto a high-resolution (50 km × 50 km) terrain model of the LIS [*Licciardi et al.*, 1998], which is similar to other 9 ka LIS topographies [e.g., *Tarasov and Peltier*, 2004]. The lapse rate adjustments only operate on the elevation differences between the coarse AOGCM topography and the higher resolution EMBM topography amounting to a mean difference of 148 ± 435 m. Varying the terrain model resolution (10 km to 100 km) does not significantly affect results (<0.0001 m yr^{-1}). AOGCMs can have positive precipitation biases along steep topography, such as the margin of an ice sheet, which would have the potential impact of biasing precipitation towards lower elevations near the ice margin. ModelE-R simulates a reduction in precipitation relative to the pre-industrial along the southwestern LIS margin at 9 ka, where the precipitation bias would presumably be the greatest, indicating that this effect is minimal in our simulations (Figures 1c and 1d).

3. Results

[6] The simulations throughout the EMBM parameter space yield a net annual 9 ka LIS surface mass balance of -0.67 ± 0.13 m yr^{-1} (the uncertainty reflecting the standard deviation of results from the Monte Carlo sampled parameter space) (Figure 2b). We focus discussion on the EMBM simulations that produced the mean LIS mass balance of -0.67 m yr^{-1}. In these mean simulations, ~36% of the LIS area is in the ablation zone (Figure 3a). Ablation generally

Table 1. Model Parameter Range

Parameter	Range
Ice Surface Roughness[a] (m)	0.01–0.05
Snow Surface Roughness[b] (m)	0.0001–0.001
Snow Albedo Decay Rate[c] (ln (°C)$^{-1}$)	−0.038–−0.045
Ice Albedo Decay Rate[c] (ln (°C)$^{-1}$)	−0.0001–−0.0009

[a]*Grainger and Lister* [1966], *Duynkerke and van den Broeke* [1994], and *Smeets and van den Broeke* [2008].
[b]*Grainger and Lister* [1966] and *Greuell and Konzelmann* [1994].
[c]*Anslow et al.* [2008].

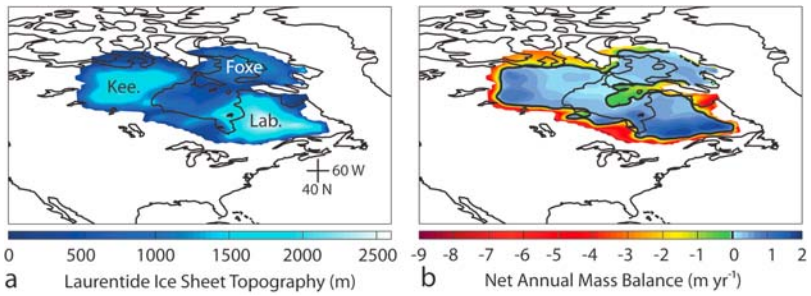

Figure 2. LIS topography [*Licciardi et al.*, 1998] and annual surface mass balance (Miller projection of maps used for comparison to Figure 1). (a) LIS topography in meters with domes labeled (Kee.=Keewatin, Lab.=Labrador). (b) LIS annual mass balance in meters water equivalent (black line denotes equilibrium line).

increases at lower elevations with the greatest mass loss rates of up to -5 m yr^{-1} along the southeast margin and -9 m yr^{-1} along the southwest margin. Accumulation areas are centered over the three LIS domes (Foxe, Keewatin, and Labrador; Figure 2) and along the saddle between the Keewatin and Labrador Domes, with rates of up to 0.8, 0.9, and 1.9 m yr^{-1} for the Foxe, Keewatin, and Labrador Domes, respectively (Figure 3). LIS equilibrium line altitudes (ELAs) range from 330 to 1,620 m, with an average ELA of ~990 m (Figure 3a and Table 2). In general, ELAs are higher along the southern, western and northwestern LIS margins than along the southeastern, eastern and northern margins and over Hudson Bay (Figures 2a and 2b). Of the three LIS Domes, the Foxe Dome has the least negative mass balance, followed by the Labrador Dome, with the Keewatin Dome having the most negative mass balance (Figures 3b–3c and Table 2). However, the Labrador Dome ELA is higher and its ablation area larger than the Keewatin Dome.

4. Discussion and Conclusions

[7] Our simulations of the 9 ka LIS mass balance are consistent with the LIS margin record. The northern margin of the Keewatin Dome and the southwestern LIS margin have the largest contiguous areas of ablation (Figure 2b). Radiocarbon dates suggest these regions rapidly deglaciated shortly after 9 ka [*Dyke*, 2004], in good agreement with the high ablation rates simulated by the EMBM. These high ablation rates are primarily in response to the high incident shortwave radiation (Figure 1a) and high summer temperatures along the LIS margins (Figure 1b) relative to the pre-industrial. A reduction in precipitation (Figure 1c) from a southward shift in the jet stream relative to the pre-industrial (Figure 1d), driven by orographic changes, likely further contributed to the negative mass balance of the southwestern LIS margin.

[8] Over Hudson Bay, the EMBM suggests a net loss of less than -1 m yr^{-1} with net gains of less than 0.5 m yr^{-1} on the saddle over southwestern Hudson Bay (Figure 2b). Combined with the ablation rates of up to -9 m yr^{-1} along the southwestern LIS margin, this imbalance would cause drawdown of the saddle over southwestern Hudson Bay in several hundred years. This likely strongly contributed to an abrupt destabilization once ice reached the ~200 m thickness required for the subglacial drainage of Lake Agassiz and attendant opening of Hudson Bay [*Clarke et al.*, 2004], in accord with radiocarbon dates that indicate the opening of Hudson Bay ~8.4 ka [*Barber et al.*, 1999].

[9] Of the three LIS domes, the Foxe Dome has the lowest average ELA and smallest ablation area (Figure 3b and Table 2), suggesting it was the most stable dome evidenced by the modern presence of ice caps and glaciers on Baffin Island. However, we likely overestimate the total Foxe Dome mass balance, as our topography does not resolve the low elevation outlet glaciers of Baffin Island [*Licciardi et al.*, 1998], whose inclusion would presumably increase ablation area and thereby decrease the net mass balance. The Keewatin Dome has a lower ELA and smaller ablation zone but also a lower mass balance than the Labrador Dome (Figure 3 and Table 2). This contrast likely reflects precipitation effects as the ablation areas of both domes have similar net melt rates (Figure 3). Large areas of the Keewatin Dome experienced a reduction in precipitation relative to the pre-industrial from the southward shift in the jet stream (Figures 1c and 1d). In contrast, precipitation increased over the southern portion of the Labrador Dome. The AOGCM simulation indicates that insolation-induced summer warming of the Northwest Atlantic, in agreement with sea surface temperature proxies [e.g., *Sachs*, 2007], and a local increase in landward wind flow may have driven

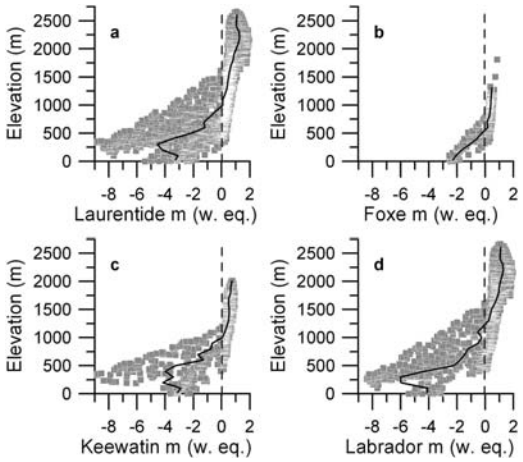

Figure 3. LIS mass balance gradients in meters water equivalent (w. eq.) for the entire (a) LIS, (b) Foxe Dome, (c) Keewatin Dome, and (d) Labrador Dome. Gray squares represent individual grid cells; black line is the average in 100 m elevation increments.

Table 2. EMBM Results

Ice Sheet/Dome	Mass Balance (m yr^{-1})	ELA (m)	ELA Range (m)	Ablation Area (%)
LIS	−0.67	990	330–1620	36
Foxe	−0.03	560	330–780	26
Keewatin	−0.85	1000	440–1200	36
Labrador	−0.77	1240	440–1620	40

greater moisture delivery from this source region to the southeastern Labrador Dome (Figures 1b–1d). The southward shift in the jet stream also likely increased moisture delivery to the southern Labrador Dome (Figure 1c). The existing southeast Labrador Dome margin chronology suggests ice may have remained close to the Northwest Atlantic for several thousand years after retreating north of the St. Lawrence River despite enhanced shortwave radiation and warmer summer temperatures along the LIS margins relative to the pre-industrial (Figures 1a and 1b) [*Dyke*, 2004; *Carlson et al.*, 2008]. We propose that the localized increase in precipitation at 9 ka may explain the persistence of the southeastern LIS margin and the Labrador Dome at lower latitudes while the LIS margin further west was rapidly retreating.

[10] The 9 ka LIS surface mass balance of -0.67 ± 0.13 m yr^{-1} translates to a sea-level rise contribution of 0.96 ± 0.19 cm yr^{-1}. By comparison, a high-resolution sea-level record indicates a rate of sea-level rise in excess of 1.2 cm yr^{-1} ~9–8.5 ka [*Cronin et al.*, 2007]. Geologic records of LIS margin retreat from 9–8.5 ka suggest a total LIS contribution to sea-level rise of $\sim 1.30 \pm 0.11$ cm yr^{-1} [*Carlson et al.*, 2008]. Surface ablation can explain 74 ± 22% (error reflects both EMBM and LIS-volume uncertainties) of the LIS mass loss during this interval with the remaining mass loss due to the dynamic processes excluded from our modeling (ice deformation, meltwater facilitated basal sliding, calving, etc.) or from an underestimation in the model of the negative surface mass balance. This study supports the hypothesis that Northern Hemisphere ice sheets can experience substantial negative surface mass balances in response to relatively small temperature (+1 to 3°C) and radiative (~20 W m^{-2}) forcings [*Carlson et al.*, 2008], with dynamic processes playing a subordinate role in ice mass loss and the disappearance of this ice sheet.

[11] **Acknowledgments.** The authors would like to thank G. Schmidt and D. Oppo for discussions of early Holocene climate, and D. Miller, P. Guest and K. Steffen for discussions. Comments and suggestions by two anonymous reviewers and the editor improved this manuscript. This research was supported by National Science Foundation Paleoclimate grants ATM-0753660 (AEC) and ATM-0753868 (ANL), UW-Madison Start-Up funds (AEC), and NASA GISS institutional support.

References

Abe-Ouchi, A., T. Segawa, and F. Saito (2007), Climatic conditions for modelling the Northern Hemisphere ice sheets throughout the ice age cycle, *Clim. Past*, *3*, 423–438.

Anslow, F. S., S. Hostetler, W. R. Bidlake, and P. U. Clark (2008), Distributed energy balance modeling of South Cascade Glacier, Washington and assessment of model uncertainty, *J. Geophys. Res.*, *113*, F02019, doi:10.1029/2007JF000850.

Barber, D. C., et al. (1999), Forcing of the cold event of 8,200 years ago by catastrophic drainage of Laurentide lakes, *Nature*, *400*, 344–348, doi:10.1038/22504.

Berger, A., and M. F. Loutre (1991), Insolation values for the climate of the last 10 million years, *Quat. Sci. Rev.*, *10*, 297–317, doi:10.1016/0277-3791(91)90033-Q.

Brook, E. J., S. Harder, J. Severinghaus, E. J. Steig, and C. M. Sucher (2000), On the origin and timing of rapid changes in atmospheric methane during the last glacial period, *Global Biogeochem. Cycles*, *14*, 559–572, doi:10.1029/1999GB001182.

Carlson, A. E., et al. (2008), Rapid early Holocene deglaciation of the Laurentide Ice Sheet, *Nat. Geosci.*, *1*, 620–624, doi:10.1038/ngeo285.

Clarke, G. K. C., D. W. Leverington, J. T. Teller, and A. S. Dyke (2004), Paleohydraulics of the last outburst flood from glacial Lake Agassiz and the 8200 BP cold event, *Quat. Sci. Rev.*, *23*, 389–407, doi:10.1016/j.quascirev.2003.06.004.

Cronin, T. M., P. R. Vogt, D. A. Willard, R. Thunell, J. Halka, M. Berke, and J. Pohlman (2007), Rapid sea level rise and ice sheet response to 8,200-year climate event, *Geophys. Res. Lett.*, *34*, L20603, doi:10.1029/2007GL031318.

Duynkerke, P. G., and M. R. van den Broeke (1994), Surface energy balance and katabatic flow over glacier and tundra during GIMEX-91, *Global Planet. Change*, *9*, 17–28, doi:10.1016/0921-8181(94)90004-3.

Dyke, A. S. (2004), An outline of North American deglaciation with emphasis on central and northern Canada, in *Quaternary Glaciations: Extent and Chronology*, vol. 2, edited by J. Ehlers and P. L. Gibbard, pp. 373–424, Elsevier, Amsterdam.

Grainger, M. E., and H. Lister (1966), Wind speed, stability and eddy viscosity over melting ice surfaces, *J. Glaciol.*, *6*, 101–127.

Greuell, W. (2000), Melt-water accumulation on the surface of the Greenland Ice Sheet: Effect on albedo and mass balance, *Geogr. Annal.*, *82*, 489–498.

Greuell, W., and T. Konzelmann (1994), Numerical modelling of the energy balance and the englacial temperature of the Greenland Ice Sheet. Calculations for the ETH-Camp location (West Greenland, 1155 m a.s.l.), *Global Planet. Change*, *9*, 91–114, doi:10.1016/0921-8181(94)90010-8.

Hansen, J., et al. (2007), Dangerous human-made interference with climate: A GISS modelE study, *Atmos. Chem. Phys.*, *7*, 2287–2312.

Holland, D. M., R. H. Thomas, B. D. Young, M. H. Ribergaard, and B. Lyberth (2008), Acceleration of Jakobshavn Isbræ triggered by warm subsurface ocean waters, *Nat. Geosci.*, *1*, 659–664, doi:10.1038/ngeo316.

Huybrechts, P., and J. deWolde (1999), The dynamic response of the Greenland and Antarctic ice sheets to multiple-century climate warming, *J. Clim.*, *12*, 2169–2188, doi:10.1175/1520-0442(1999)012<2169:TDROTG>2.0.CO;2.

Indermühle, A., et al. (1999), Holocene carbon-cycle dynamics based on CO_2 trapped in ice at Taylor Dome, Antarctica, *Nature*, *398*, 121–126, doi:10.1038/18158.

Joughin, I., W. Abdalati, and M. Fahnestock (2004), Large fluctuations in speed of Greenland's Jakobshavn Isbræ glacier, *Nature*, *432*, 608–610, doi:10.1038/nature03130.

Joughin, I., et al. (2008), Seasonal speedup along the western flank of the Greenland Ice Sheet, *Science*, *320*, 781–783, doi:10.1126/science.1153288.

LeGrande, A. N., and G. A. Schmidt (2009), Sources of Holocene variability of oxygen isotopes in paleoclimate archives, *Clim. Past*, *5*, 441–455.

Licciardi, J. M., P. U. Clark, J. W. Jenson, and D. R. Macayeal (1998), Deglaciation of a soft-bedded Laurentide Ice Sheet, *Quat. Sci. Rev.*, *17*, 427–448, doi:10.1016/S0277-3791(97)00044-9.

Luckman, A., T. Murray, R. deLange, and E. Hanna (2006), Rapid and synchronous ice-dynamic changes in East Greenland, *Geophys. Res. Lett.*, *33*, L03503, doi:10.1029/2005GL025428.

Marshall, S. J., T. S. James, and G. K. C. Clarke (2002), North American Ice Sheet reconstructions at the Last Glacial Maximum, *Quat. Sci. Rev.*, *21*, 175–192, doi:10.1016/S0277-3791(01)00089-0.

Meehl, J. H., et al. (2007), Global climate projections, in *Climate Change 2007: The Physical Science Basis. Contribution of Working Group I to the Fourth Assessment Report of the Intergovernmental Panel on Climate Change*, edited by S. Solomon et al., pp. 748–845, Cambridge Univ. Press, New York.

Mitchell, J. F. B., N. S. Grahame, and K. J. Needham (1988), Climate simulations for 9000 years before present: seasonal variations and effect of the Laurentide Ice Sheet, *J. Geophys. Res.*, *93*, 8283–8303, doi:10.1029/JD093iD07p08283.

Nick, F. M., A. Vieli, I. M. Howat, and I. Joughin (2009), Large-scale changes in Greenland outlet glacier dynamics triggered at the terminus, *Nat. Geosci.*, *2*, 110–114, doi:10.1038/ngeo394.

Pfeffer, W. T., J. T. Harper, and S. O'Neel (2008), Kinematic constraints on glacier contributions to 21st-century sea-level rise, *Science*, *321*, 1340–1343, doi:10.1126/science.1159099.

Pollard, D., and PMIP Participation Groups (2000), Comparisons of ice-sheet surface mass budgets from Paleoclimate Modeling Intercomparison Project (PMIP) simulations, *Global Planet. Change*, *24*, 79–106, doi:10.1016/S0921-8181(99)00071-5.

Pollard, D., J. C. Bergengren, L. M. Stillwell-Soller, B. Felzer, and S. L. Thompson (1998), Climate simulations for 10000 and 6000 years BP using the GENESIS Global Climate Model, *Paleoclimates*, *2*, 183–218.

Pritchard, H. D., R. J. Arthern, D. G. Vaughan, and L. A. Edwards (2009), Extensive dynamic thinning on the margins of the Greenland and Antarctic ice sheets, *Nature*, *461*, 971–975, doi:10.1038/nature08471.

Rignot, E., and P. Kanagaratnam (2006), Changes in the velocity structure of the Greenland Ice Sheet, *Science*, *311*, 986–990, doi:10.1126/science.1121381.

Sachs, J. P. (2007), Cooling of northwest Atlantic slope waters during the Holocene, *Geophys. Res. Lett.*, *34*, L03609, doi:10.1029/2006GL028495.

Shepherd, A., A. Hubbard, P. Nienow, M. King, M. McMillan, and I. Joughin (2009), Greenland Ice Sheet motion coupled with daily melting in late summer, *Geophys. Res. Lett.*, *36*, L01501, doi:10.1029/2008GL035758.

Smeets, C. J. P. P., and M. R. van den Broeke (2008), Temporal and spatial variations of the aerodynamic roughness length in the ablation zone of the Greenland Ice Sheet, *Boundary Layer Meteorol.*, *128*, 315–338, doi:10.1007/s10546-008-9291-0.

Sowers, T., R. B. Alley, and J. Jubenville (2003), Ice core records of atmospheric N_2O covering the last 106,000 years, *Science*, *301*, 945–948, doi:10.1126/science.1085293.

Tarasov, L., and W. R. Peltier (2004), A geophysically constrained large ensemble analysis of the deglacial history of the North American ice sheet complex, *Quat. Sci. Rev.*, *23*, 359–388, doi:10.1016/j.quascirev.2003.08.004.

Zwally, H. J., et al. (2002), Surface melt-induced acceleration of Greenland Ice-Sheet flow, *Science*, *297*, 218–222, doi:10.1126/science.1072708.

F. S. Anslow, Earth and Ocean Sciences, University of British Columbia, Vancouver, BC V6T 1Z4, Canada.

A. E. Carlson, E. A. Obbink, and D. J. Ullman, Department of Geoscience, University of Wisconsin-Madison, Madison, WI 53706, USA. (acarlson@geology.wisc.edu)

A. N. LeGrande, NASA Goddard Institute for Space Studies, Columbia University, New York, NY 10025, USA.

J. M. Licciardi, Department of Earth Sciences, University of New Hampshire, Durham, NH 03824, USA.